Georgios SAVAIDIS* and Timm SEEGER**

Material Behaviour and Life Evaluation under Cyclic Multiaxial Proportional Loading

* MAN Nutzfahrzeuge AG, Dep. TEB, Dachauerstr. 667, 80995 Munich-Germany

** Fachgebiet Werkstoffmechanik, THD, Petersenstr. 13, 64283 Darmstadt-Germany

Keywords: Multiaxiality, material behaviour, crack closure, variable amplitudes

ABSTRACT: In this paper the results of fatigue tests under fully reversed axial, torsional and combined (axial + torsional) strain controlled loading are presented and discussed, determined with thin-walled tube specimens of FeE460 and Al5083. Fatigue results on uniaxially loaded standardized hourglass specimens have also been conducted to study effects resulting from the different specimen shape. Cyclic deformation under proportional loading can be described uniformly by the stabilized σ-ε *curve if stresses and strains are expresssed as equivalent values according to the von Mises criterion. Failure behaviour is characterized by the growth of short surface cracks at right angles to the direction of the highest principal stress under pure axial and combined loading. In the case of torsional loading the crack growth occurs parallel to both shear stress directions. The comparison of the experimental results with predicted fatigue life curves for CA and VA loading with various multiaxiality ratios using a new fracture mechanics based model demonstrates the improvement in fatigue life evaluation.*

Notation

a, 2a	depth and length of a semi-circular surface crack, respectively
A_5	elongation at fracture
b	fatigue strength exponent
c	fatigue ductility exponent
CA	constant amplitude
E	Young´s modulus
H_0	magnitude of load spectrum
I	irregularity factor
K´	cyclic hardening coefficient
K_t	notch concentration factor
n, N	number of cycles and number of cycles to failure, respectively
n´	cyclic hardening exponent
R	nominal stress ratio
$R_{p0,2}$, R_m	yield stress with 0.2% offset and ultimate tensile strength, respectively

VA	variable amplitude
γ	shear strain
ΔJ	range of the cyclic J-integral
ε	axial strain
$\varepsilon_1, \varepsilon_2, \varepsilon_3$	principal tensile strains
ε_f'	fatigue ductility coefficient
λ, Λ	strain proportionality ratio and principal stress ratio, respectively
ν, ν'	Poisson's ratio and elasto-plastic Poisson's ratio, respectively
σ	axial stress
σ_1, σ_2	principal tensile stresses
σ_f'	fatigue strength coefficient
τ	shear stress
Subscripts	
a	amplitude
eff	effective
eq	equivalent
E	endurance
x, y	coordinates

Introduction - Background

The calculation of fatigue life to initiation of cracks of technical size ($2a \approx 0.5$mm) in engineering components using the Local Strain Approach needs secured knowledge of (a) the relation between the applied loads and the local stresses and strains, and (b) the deformation and the failure behaviour of the stressed material. The latter task is quite difficult, especially in the case of VA loading when load sequence effects significantly influence the fatigue process. This is one of the main reasons why life calculations supported by conventional mean stress parameters often deviate from experimental results.

For uniaxial loading cases, Vormwald has demonstrated that elasto-plastic fracture mechanics combined with the closure concept offers an efficient tool for improving the accuracy of fatigue life evaluation, covering both mean stress and load sequence effects (1, 2). For multiaxial loading cases several parameters are reported in the literature; these describe the material deformation when both shear and axial stress amplitudes as well as mean stress effects are acting, but load sequence effects during a VA loading history can not be considered.

A main handicap to further development of Vormwald's model to multiaxial loading was that only a few experimental results giving essential information on the

phenomenon of load sequence effects at various multiaxiality ratios were reported in the literature. Starting from this point, an experimental investigation program has been performed on unnotched specimens from two materials, loaded under constant and variable amplitudes with various ratios of multiaxiality. This paper gives details of the performance of the tests and the essential findings.

Based on Vormwald's procedure a fracture mechanics based model has been developed, predicting the fatigue life to initiation of cracks of a length 2a≈0.5mm in the notch root of engineering components under multiaxial, proportional loading (3, 4). Mean stresses and load sequence effects are explicitly considered. The experimental results are used to demonstrate the improvement in fatigue life calculation using the new model.

Test Materials

Two materials were investigated: (a) the micro alloyed fine grained FeE460 steel and (b) the (weldable) aluminum alloy Al5083. The chemical composition and monotonic material properties are compiled in Tables 1 and 2, respectively. The test specimens were machined out of 100mm thick plates. The specimen axis was always parallel to the rolling direction. FeE460 shows a ferrite-perlite microstructure with about 80% of ferrite. The average grain size is about 10µm. Al5083 shows an α-mixed crystal with β-segregations of Al_3Mg_2. Typical pancake-shaped grains are observed with an average extension of the long side of 80µm.

Table 1. Chemical composition of FeE460 and Al5083 in [%] as declared by the manufactures.

Material	C	Si	Mn	P	S	Al	Cr	Mo	Mg	Ti
FeE460	0.18	0.44	1.54	0.016	0.001	0.013	0.022	0.004		
Al5083		0.12	0.67			Rest	0.063		4.67	0.014

Material	Ni	V	Fe	N	Zn
FeE460	0.27	0.17	Rest	0.019	
Al5083					0.031

Table 2. Monotonic material properties of FeE460 and Al5083.

MATERIAL	E N/mm^2	$R_{p,0.2}$ N/mm^2	R_m N/mm^2	A_5 %
FeE460	208500	500	643	26.2
Al5083	68000	169	340	20.2

Test specimens

All tests under torsional and combined (axial+torsional) strain controlled loading were performed with thin-walled tube specimens, in order to guarantee an approximately uniform stress and strain distribution of the highest stressed material section for both materials investigated. Axial tests were performed with standard smooth hourglass shaped specimens. Some axial tests were conducted with thin-walled tube specimens in order to study effects resulting from the different specimen shape.The specimens used are shown in Fig. 1.

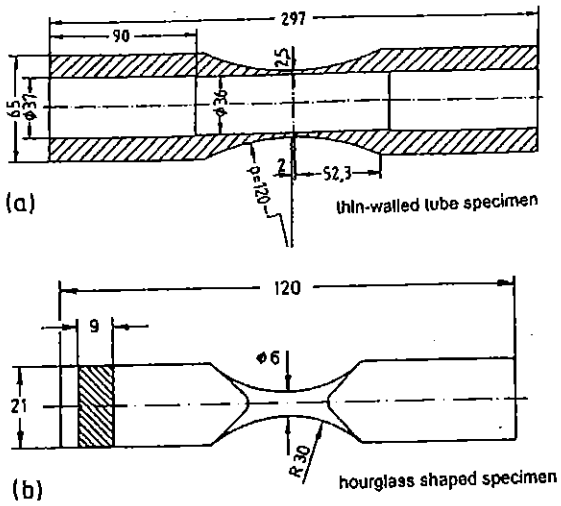

Fig. 1 Test specimens

Fatigue test program

Strain controlled fatigue tests with fully reversed constant and variable amplitudes and various strain proportionality ratios $\lambda=\gamma/\varepsilon$ were performed. For both CA and VA loading the strain proportionality ratios were $\lambda=0$ (axial), $\lambda=\infty$ (torsional) and $\lambda=\sqrt{3}$ (axial + torsional). Additionally, tests at $\lambda=0$ were performed on hourglass shaped specimens. The failure criterion was the formation of a surface crack of length $2a\approx0.5$-0.6mm.

Under VA loading, the fatigue lives were determined for random sequences using the method of notch strain simulation (5). With this, the load sequence in nominal stress of a fictitious notched specimen is transformed into the strain sequence of the notch root element using the tools of the Local Strain Approach. For multiaxial proportional loading these tools are the equations of Hoffmann and Seeger (6). The calculated strain sequences are then forced on to an unnotched specimen. Note that the fulfilment of the equivalence principle (size, gradient effects, etc.) between the used unnotched specimen and the notch root material behaviour is not of any relevance to the results of the present investigation. The fictitious notched shaft used in this investigation is plotted in Fig. 2. It is subjected to fully reversed axial, torsional and combined nominal stress gaussian spectrum loading with a magnitude of 10^5 cycles, an irregularity factor of 0.99. The corresponding notch stress concentration factors for the various loading situations are given in Fig. 2.

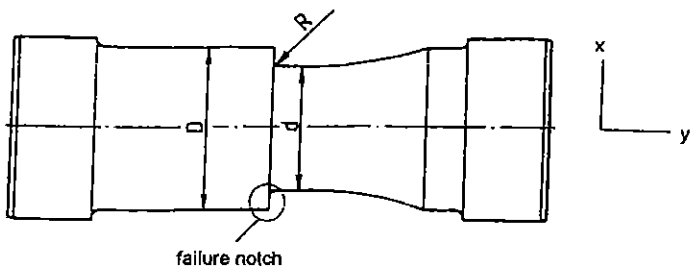

$\frac{D}{d}=1.3 \quad \frac{R}{d}=0.05 \quad K_{t,y}=2.22 \quad K_{t,x}=0.34 \quad K_{t,xy}=1.6$

Fig. 2. Fictitious notch shaft for the notch strain simulation

Results

Deformation behaviour

The materials used exhibit a completely different deformation behaviour under cyclic loading. Fig. 3 shows exemplary cyclic deformation curves of both materials determined for various equivalent strain amplitudes $\varepsilon_{eq,a}$ and all three proportionality ratios λ. Please note that stress-strain paths were not recorded completely so that some of the plotted curves end at cycle numbers smaller than the corresponding failure criterion.

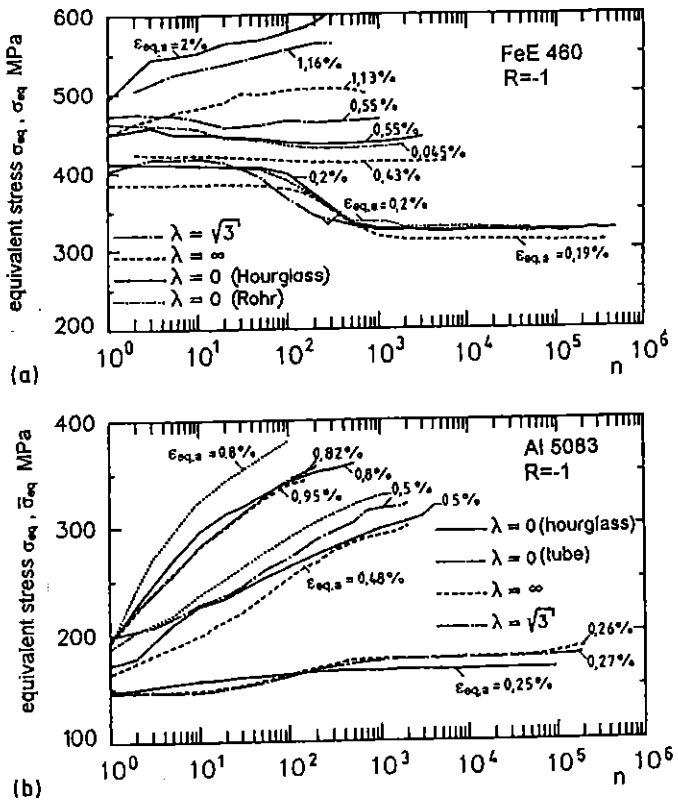

Fig. 3. Cyclic deformation curves of (a) FeE460 and (b) Al5083 at various λ-ratios.

The equivalent stress amplitudes are estimated using the von Mises criterion:

$$\sigma_{eq,a} = \sqrt{\sigma_a^2 + 3\tau_a^2} \tag{1}$$

The values of shear strain γ and/or axial strain ε are constant, while the values of shear stress τ and axial stress σ are measured during each fatigue test. The equivalent strain amplitude under tensional or combined loading is calculated using Hencky´s equations, which express the relation between the components and the corresponding equivalent values:

$$\gamma_a = 2\,(1+\nu')\,\frac{\varepsilon_{eq,a}}{\sigma_{eq,a}}\,\tau_a \tag{2}$$

$$\nu' = \frac{1}{2} - \left(\frac{1}{2} - \nu\right)\frac{\sigma_{eq,a}}{E\,\varepsilon_{eq,a}} \tag{3}$$

In Eqs. (2) and (3) the unknown variables are $\varepsilon_{eq,a}$ and ν'. The equivalent stress amplitude $\sigma_{eq,a}$ is to be calculated using Eq. (1). In cases where the stress values are not known, $\varepsilon_{eq,a}$ can be estimated depending on the principal strain values using Eq. (4).

$$\varepsilon_{eq,a} = \frac{1}{\sqrt{2}\,(1+\nu)}\sqrt{(\varepsilon_{1,a}-\varepsilon_{2,a})^2 + (\varepsilon_{1,a}-\varepsilon_{3,a})^2 + (\varepsilon_{2,a}-\varepsilon_{3,a})^2} \tag{4}$$

The principal strains ε_1, ε_2, ε_3 can be calculated depending on ε and γ.

Al5083 shows a strain hardening behaviour at all load levels and proportionality ratios investigated. With increasing strain amplitude the hardening behaviour increases. Cyclic stabilization is observed only at low equivalent strain values. FeE460 exhibits a strain amplitude-depending deformation behaviour: strain hardening at high equivalent strain levels and strain softening at lower equivalent strain values. Cyclic stabilization can be observed in nearly all the cases investigated.

The stabilized stresses for the applied strain amplitudes, or - in cases of no stabilization - the corresponding values at 50% of the fatigue life, are of special in-terest because they are used as input for calculations using the Local Strain Approach. Fig. 4 shows all experimental stress-strain results for both materials measured at half fatigue life. The curves have been determined using regression analysis of the results from the hour-glass specimens at λ=0 for a probability of survival of 50%. It can be recognized that results for all λ values and both materials can be accurately described with the corresponding curves for uniaxial loading. These findings correlate well with experimental results from other materials reported from Reininghaus (7), Fatemi (8) and Sonsino (9). The curves are

described with the Ramberg-Osgood relation:

$$\varepsilon_{eq,a} = \frac{\sigma_a}{E} + \left(\frac{\sigma_a}{K'}\right)^{1/n'} \tag{5}$$

The values of K´ and n´ of both materials are compiled in Table 3.

Table 3. Cyclic properties of FeE460 and Al5083.

Material	ε_E	K´	n´	σ_f'	b	ε_f'	c
	%	N/mm^2					
FeE460	0.173	1115	0.161	969.6	-0.086	0.281	-0.493
Al5083	0.222	544	0.075	780.3	-0.114	1.153	-0.861

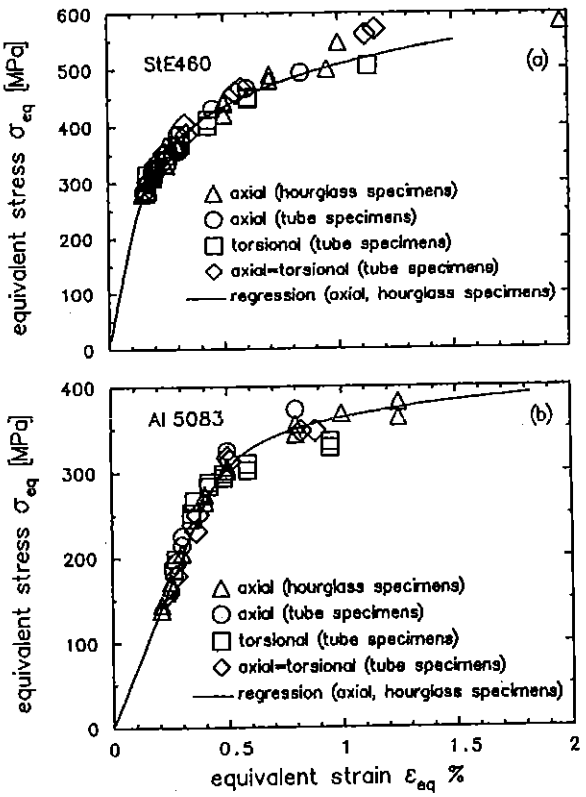

Fig. 4. Stabilized σ_{eq}–ε_{eq}-levels of (a) FeE460 and (b) Al5083 at various λ values.

For both materials no significant influence of the different specimen shape on the deformation behaviour has been detected.

Failure behaviour

The failure behaviour depends strongly on the applied strain amplitude and the strain proportionality ratio for both materials investigated. Under axial or combined (axial + torsional) loading and low strain levels failure occurs with the initiation and growth of one microcrack till the failure criterion of a surface crack length of 0.5-0.6mm is reached. Under higher strain levels many microcracks could be detected which coalesce to larger cracks during the cyclic loading.

Under axial loading the cracks were orientated perpendicular to the specimen axis and loading direction (mode I cracks). Under combined loading with $\lambda=\sqrt{3}$ the crack were observed to grow at angles of 110°-125° in relation to the specimen axis, approximately perpendicular to the direction of the highest principal stress (mode I cracks) calculated at 30°.

Under pure torsional loading the detected microcracks grew parallel or perpendicular to the specimen axis, which corresponds to the directions of the shear stresses, for both materials. The crack tips at the specimen surface are subject to a mode II loading situation. When the cracks reached lengths much greater than the failure criterion (long cracks) they turned, growing at 45° in relation to the specimen axis (mode I).

The fatigue life results for failure crack lengths of 2a=0.5-0.6mm under CA and VA loading for various λ values are plotted in Figs 5a and 5b for FeE460 and Al5083, respectively. The curves plotted with thin lines have been obtained to adapt the results determined from hourglass specimens under CA loading with $\lambda=0$ using regression analysis for a probability of survival of 50%. The endurance limit was calculated using the maximum-likelihood method. The curves are described using the Manson-Coffin-Morrow relationship:

$$\varepsilon_{eq,a} = \frac{\sigma_f'}{E}(2N)^b + \varepsilon_f'(2N)^c \qquad (6)$$

The material constants σ_f', ε_f', b and c are listed in Table 3.

The deviations between the results from the thin-walled specimens and those from the hourglass specimens at λ=0 indicate the influence of the different specimen shape on the failure behaviour. Thin-walled tube specimens show buckling effects observed optically during the tests. These effects are more significant with increasing ε_a levels and decreasing λ values (higher compression force). Hourglass specimens are not sensitive to buckling effects (within the tested loading amplitudes), and so the fatigue life results for λ=0 are of about the same values as those under torsional or combined loading of the thin-walled specimens. The experimental results for both materials indicate that fatigue life evaluation under CA fully reversed loading can be performed uniformly for various λ ratios using the equivalent stress and strain calculated according to the von Mises criterion.

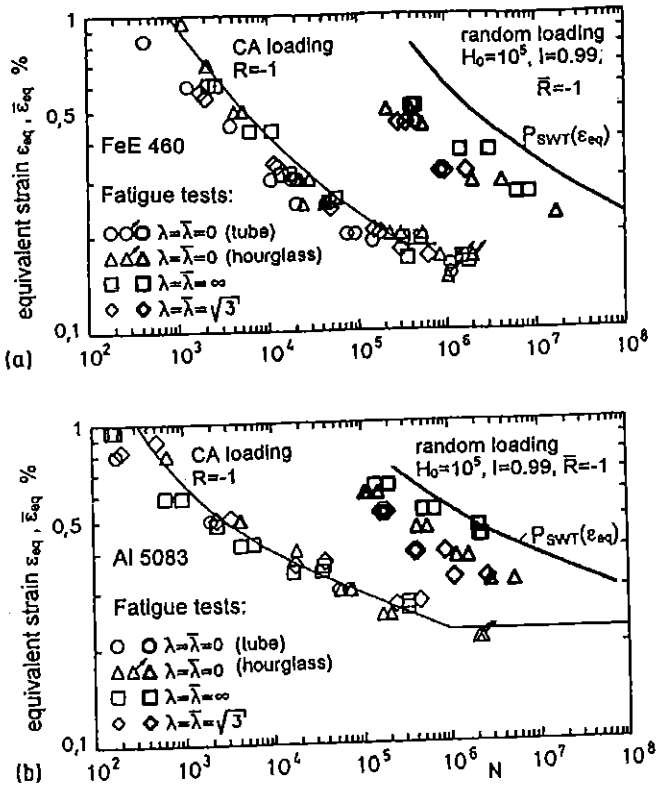

Fig. 5. Test results for CA and VA loading compared to calculated fatigue lives using the Local Strain Approach supported by $P_{SWT}(\varepsilon_{eq})$. (a) FeE460, (b) Al5083.

The same failure behaviour in respect of crack orientation for the various λ values has been observed under VA loading, too. The corresponding fatigue lives for both materials are plotted in Figs. 5a and 5b versus the greatest equivalent strain value $\varepsilon_{eq,a}$ during the load histories using bold symbols. It can further be recognized that the fatigue life curves for both materials, evaluated with the Local Strain Approach using an equivalent strain supported P_{SWT}-N-curve, deviate significantly from the corresponding experimental results. This phenomenon is well known for uniaxial loading cases. It is to be explained with load sequence effects which have a reducing influence on fatigue life. The experimental results at $\lambda=0$, $\lambda=\sqrt{3}$ and $\lambda=\infty$ fall into a uniform „scatter" band, indicating that such effects exist also at multiaxial loading. They are of less significance in the case of pure torsional loading, where mode II crack propagation occurs at the specimen surface, compared to the other investigated load configurations.

Remarks

The essential findings of the experimental investigation on specimens of FeE460 and Al5083 are:

1. Deformation behaviour under multiaxial proportional loading can be described uniformly using the uniaxial σ–ε-curve if stresses and strains are expressed in equivalent values using the von Mises criterion.
2. Multiaxial proportional CA or VA loading yields crack propagation perpendicular to the direction of the highest principle stress (mode I propagation) in the cases of axial and combined loading. Under pure torsional loading the cracks are orientated parallel to the directions of the shear stresses (mode II propagation at the specimen surface).
3. Fatigue lives under *fully reversed CA* loading can be described uniformly using the equivalent strain. Note that the efficiency of ε_{eq} for describing the influence of the loading *amplitude* on multiaxial fatigue behaviour is restricted. Difficulties or inaccuracies in the use of ε_{eq} may result if (a) mean stresses or (b) variable amplitude loading histories or (c) a combination of both, mean stresses and variable amplitudes, are acting. The difficulty if mean stresses are acting is that equivalent strains are always calculated with positive signs without regard to the sign of the axis stress (e.g. compression and

tensional stresses of the same value yield the same equivalent strain). A solution for avoiding this obstacle is suggested by Sonsino (10) transforming the mean stress affected hysteresis loops into those causing the same damage and exhibiting no mean stresses using Haigh diagrams developed for each material and individual λ-values. Note, that if such Haigh-diagrams are not available their development would require great experimental effort. In such cases, the use of conventional parameters for multiaxial loading reported in the literature (see the overviews given by Garud (11) and Vormwald and Bergmann (12)) within the framework of the Local Strain Approach is recommended. These parameters have been developed on the basis of corresponding experimental results for CA loading and would therefore allow a consistent treatment of mean stresses and reliable fatigue life approximations at CA loading. At VA loading, however, where load sequence effects influence the fatigue life, the use of these parameters would yield inaccurate approximations. This can be easily recognized when the special case of uniaxial loading is treated. More detailed discussion on mean stress consideration in fatigue life calculation is given in Ref. (13).

P_J-Parameter

Using elasto-plastic fracture mechanics Vormwald (1, 2) described the closure and propagation behaviour of short cracks under *uniaxial* loading covering both mean stress and load sequence effects. The implementation of Vormwald's procedure within the framework of the Local Strain Approach yielded an improvement in fatigue evaluation. Additional investigations made by the authors were dedicated to extending Vormwald's procedure to multiaxial loading cases. In the special case of multiaxial *proportional* loading this has been recently performed in Ref. (3, 4). Compared to Vormwald's procedure the model developed is characterized by two main features: (a) the use of Hoffmann's and Seeger's equations (6) to describe the proportional stress-strain path and (b) the damage caclulation of the stress-strain path considering the influence of multiaxiality on both the closure and propagation behaviour of (engineering) short cracks. For this, a parameter P_J^{multi} has been defined

$$P_J^{multi} = \frac{\Delta J_{eff}^{multi}}{a}. \qquad (7)$$

In Eq. (7) ΔJ_{eff} is the effective range of the J-integral as developed by He (14) and Dowling (15) for mixed mode and mode I loading, respectively. The superscipt „multi" indicates the multiaxial state of loading. The effective values of stresses and strains are calculated using Newman's crack opening equations for uniaxial loading (16), simply modified to consider multiaxial loading conditions. For this, third-degree polynomian relationships have been developed on the basis of numerical results from McClung (17) determined on a biaxial loaded mode I crack. Details about the development of P_J^{multi} for various crack types and load configurations and its implementation into the Local Strain Approach are given in Ref. (4).

Note that the relationships calculating the effective stresses within the framework of P_J^{multi} have been developed using data for mode I propagation. Therefore, the parameter considers physically reasonable mean stresses and load sequence effects for various multiaxility ratios when mode I propagation occurs ($\lambda \neq \infty$). In the case of mode II propagation ($\lambda = \infty$) the authors suggest that purly formally the same relationships be used to calculate the effective stresses (since at the moment no relationships estimating crack opening and closure levels at mode II propagation exist in the literature), taking into consideration that this will yield conservative approximations of the effective stress values.

Experimental verification

The experimental fatigue lives determined with the specimens of FeE460 and Al5083 under CA and VA loading at $\lambda = 0$, $\sqrt{3}$ and ∞ have been used to check the prediction accuracy of the developed model. Fig. 6 and Fig. 7 show the results for both materials. The experimental results correspond to final surface crack lengths of $2a \approx 0.5$-0.6mm. The predictions have been performed assuming a semi-circular surface crack type with a failure surface crack length of $2a = 0.5$mm. The (fictitious) starting crack lengths were calculated to 15µm and 31µm for FeE460 and Al5083, respectively.

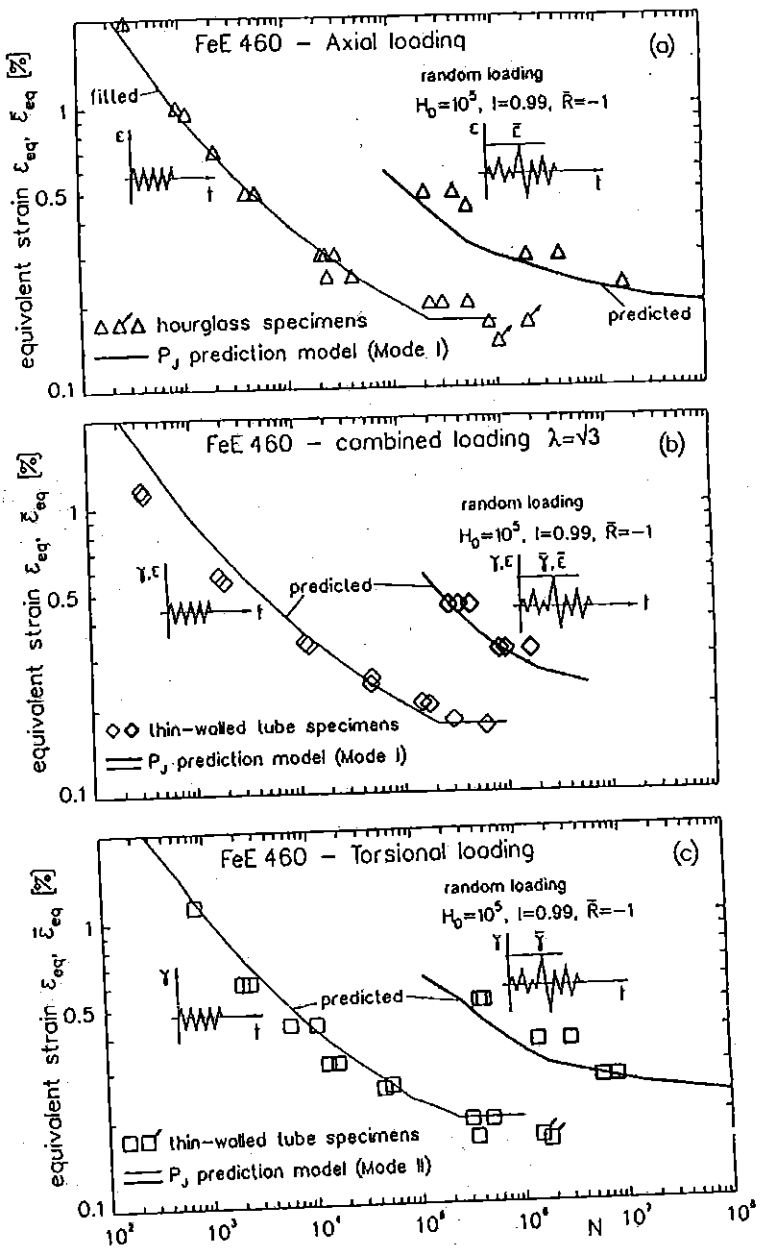

Fig. 6. Comparison of test results at (a) axial, (b) combined, and (c) torsional loading with fatigue life curves predicted using the Local Strain Approach supported by P_J^{multi} for FeE460.

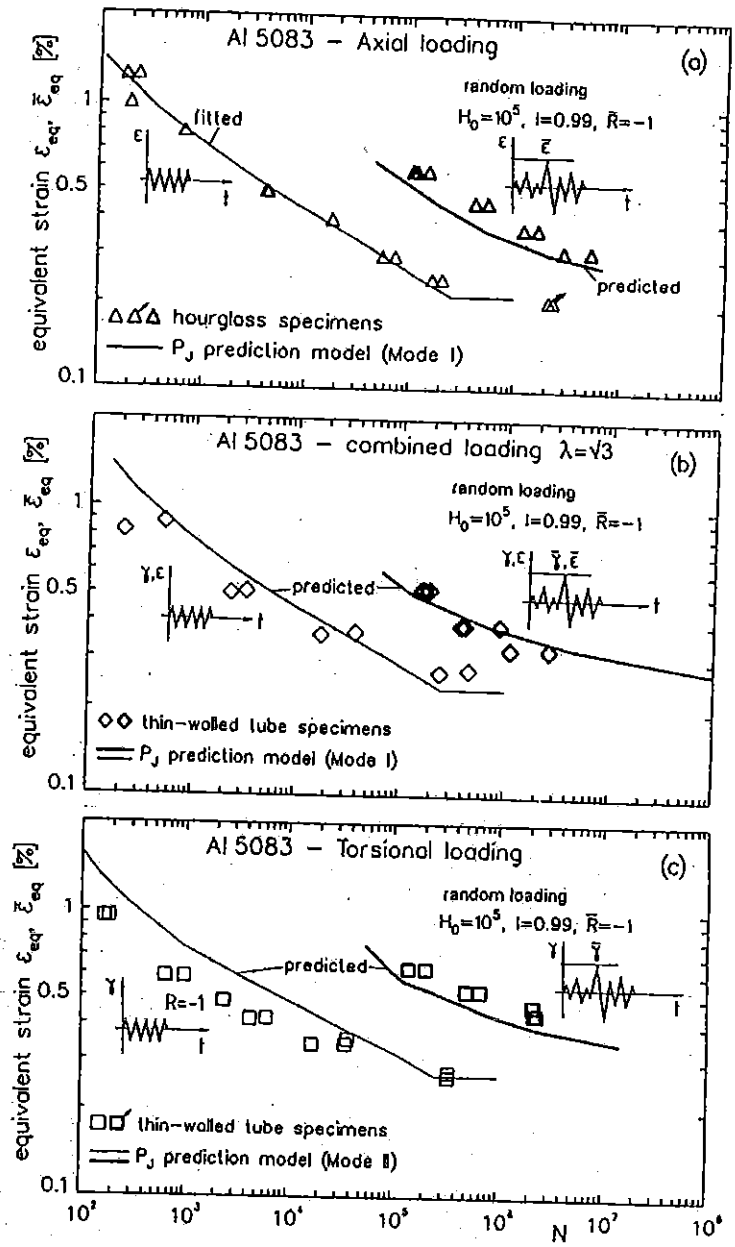

Fig. 7. Comparison of test results at (a) axial, (b) combined, and (c) torsional loading with fatigue life curves predicted using the Local Strain Approach supported by P_J^{multi} for Al5083.

For multiaxial proportional loading cases yielding mode I crack propagation behaviour (λ=0, $\sqrt{3}$) the P_J^{multi} relationship developed in Ref. (3) for a semi-circular surface crack is:

$$P_J^{multi,I} = \left(\Delta\sigma_{1,eff}\right)^2 \left[1.364 \frac{1-\nu^2}{E} + 1.023 \frac{2}{\sqrt{n'}} \left(\frac{1}{2K'} \right)^{1/n'} \left(\Delta\sigma_{1,eff} \sqrt{1-\Lambda+\Lambda^2} \right) \right] \qquad (8)$$

where $\Lambda = \sigma_2 / \sigma_1$. For torsional loading yielding mode II propagation behaviour the P_J^{multi} relationship for the crack tips at the specimen surface is given with Eq. (9):

$$P_J^{multi,II} = \frac{\Delta\sigma_{1,eff}}{(2-\nu)^2} \left\{ 6.677 \frac{\Delta\sigma_{1,eff}}{E} + 9.512 \frac{2}{\sqrt{n'}} \left(\frac{\Delta\sigma_{1,eff}\sqrt{3}}{2K'} \right)^{\frac{1}{n'}} \right\} \qquad (9)$$

The superscripts I and II in Eqs. (8) and (9), respectively, indicate the individual crack propagation mode. The values of the coefficients and the algorithms to calculate $\Delta\sigma_{1,eff}$ depending on the load history in Eqs. (8) and (9) are described in detail in Ref. (4). The results for axial loading (mode I propagation) are plotted in Figs. 6(a) and 7(a) for both materials. Notice that the thin lines have been obtained to adapt the corresponding experimental results for CA loading using regression analysis. Under VA loading, the predicted fatigue lives are shorter than the experimentally determined ones for both materials, indicating the already known tendency to overestimate load sequence effects (1, 2). The predicted and experimental results for combined loading (mode I propagation) are plotted in Figs 6(b) and 7(b) for FeE460 and Al5083, respectively. The prediction accuracy is satisfactory under both CA and VA loading. The slight deviations between predicted and experimental results at high equivalent strain values (CA loading) are to be explained by buckling effects of the thin-walled specimens used. These effects have been observed optically during the tests.

The fatigue lives for torsional loading (mode II propagation at the specimen surface) are plotted in Figs 6(c) and 7(c) for both materials. The prediction accuracy is satisfactory under both CA and VA loading, especially for FeE460, though the (conservative) evaluation of the effective cycles using the developed crack opening stress equations based on mode I propagation does not conform to the experimentally observed mode II propagation. A deviation of a factor of 3-5 between predicted and experimental

fatigue lives can be observed for Al5083 under CA loading. An explanation for this could possibly be the fact that small inaccuracies in the estimation of $P_J^{multi,II}$ (occurring from Newman´s modified crack opening stress equations in connection with the different mode propagation behaviour) yield large inaccuracies in the predicted fatigue lives because of the quite flat slope of the fatigue life curve for this material.

Conclusions

Deformation behaviour of FeE460 and Al5083 under multiaxial proportional loading can be described uniformly using the uniaxial σ–ε-curve if stresses and strains are expressed in equivalent values. Failure behaviour is characterized by mode I crack growth in the case of axial and combined loading. Under torsional loading mode II short crack propagation has been observed at the specimen surface.

Life predictions using the Local Strain Approach supported by P_J^{multi} coincide well with the experimental results in most of the cases investigated. The known tendencies in the influence of multiaxiality, load sequence and mean stresses are described reasonable, except for the procedure for calculating opening stress-strain values when mode II-crack propagation occurs. Therefore, additional experimental investigations should be performed to develop equations describing physically reasonable mode II and mixe mode crack opening behaviour. Furthermore, the prediction accuracy of the procedure presented must be checked using experimental results from notched components and/or other materials than those investigated here. In addition, analytical and experimental work should be dedicated to extending the applicability of P_J^{multi} to multiaxial-nonproportional load configurations. Here it is suggested that the application of P_J^{multi} to nonproportional *synchronous* loading cases be performed next. A corresponding analytical procedure to describe the stress-strain behaviour, which can be directly implemented into the Local Strain Approach, has been developed in Ref (18).

References

(1) Vormwald M. and Seeger T., (1991), The consequences of short crack closure on fatigue crack growth under variable amplitude loading. Fatigue Frac. Engng Mater. Struct., vol. 14, p.205-225.

(2) Vormwald M. and Heuler P. and Seeger T., (1992), A fracture mechanics based model for cumulative damage analysis as part of fatigue life prediction. In: Advances in Fatigue Lifetime Predictive Techniques, ASTM STP 1122, (Edited by M.R. Mitchell and R.W. Landgraf), Philadelphia, pp.28-43

(3) Savaidis G. and Seeger T., (1996), A short crack growth prediction model for multiaxial proportional elasto-plastic loading. In: Fatigue 96, Proc. of the 6th Int. Fatigue Congress, (Edited by G. Lütjering and H. Nowack), vol. II, Berlin, pp.1001-1006.

(4) Savaidis G. and Seeger T., (1997), Consideration of multiaxiality in fatigue life prediction using the closure concept. Fatigue Frac. Engng Mater. Struct., to be published.

(5) Heuler P. and Seeger T., (1984), Notch simulation concepts for the evaluation of crack initiation lives of service loaded components. In: Proc. of Fatigue 84, Birmingham, pp.1741-1752.

(6) Seeger T. and Beste A., (1977), Zur Weiterentwicklung von Näherungsformeln für die Berechnung von Kerbbeanspruchungen im elastisch-plastischen Bereich. In: Kerben und Bruch, VDI-Fortschrittsberichte, Reihe 18, No. 2.

(7) Reininghaus M., (1994), Baustahl St52 unter zweiachsiger plastischer Wechselbeanspruchung. Universität Carolo-Wilhelmina, Braunschweig, phd-thesis.

(8) Fatemi A., (1989), Biaxial fatigue of 1045 steel under in-phase and 90 deg out-of-phase loading conditions. In: Multiaxial Fatigue. Analysis and Experiments, (Edited by G.E. Leese and D. Socie). SAE AE-14, pp.121-137.

(9) Sonsino C.M., (1995), Multiaxial fatigue of welded joints under in-phase and out-of-phase local stresses and strains. Int. J. of Fatigue, vol. 17, p.55-69.

(10) Sonsino C.M., (1994), Schwingfestigkeit von geschweißten Komponenten unter komplexen elasto-plastischen, mehrachsigen Verformungen. LBF-Nr. 6078, Fraunhofer Institut für Betriebsfestigkeit.

(11) Garud Y.S., (1981),. Multiaxial fatigue. A survey of the state of art. J. of Testing and Evaluation, vol. 9, p.165-178.

(12) Vormwald M. and Bergmann J., (1990), Entwicklung eines strukturabhängigen Werkstoffmodells für komplexe Hochtemperaturbeanspruchungen. Forschungsbericht IABG-BMFT.

(13) Savaidis G. and Seeger T., (1996), Deformation und Versagen von StE460 und AlMg4,5Mn bei mehrachsig-proportionalen Beanspruchungen mit konstanten und variablen Amplituden. Materialwissenschaft und Werkstofftechnik, Heft 9, p.444-452.

(14) He M.Y., (1987), Perturbation solutions on *J*-integral for nonlinear crack problems. J. of Appl. Mech., vol. 54, p.240-242.

(15) Dowling N.E., (1987), J-integral estimates for cracks in infinite bodies. Eng. Frac. Mech., vol. 223, p.333-348.

(16) Newman J.C., (1984), A crack opening stress equation for fatigue crack growth. Int. J. of Frac., vol. 24, p.R131-R135.

(17) McClung R.C., (1993), Finite element modelling of fatigue crack growth. In: Theoretical Concepts and Numerical Analysis of Fatigue, (Edited by A.F. Blom and C.J. Beevers), pp.153-171.

(18) Savaidis A., (1994), Finite-Element Untersuchungen und Entwicklung eines Näherungsverfahrens zur Beschreibung mehrachsiger elastisch-plastischer Kerbbeanspruchungen bei synchroner nichtproportionaler zyklischer Belastung. Institut für Stahlbau und Werkstoffmechanik der TH Darmstadt, Heft 52.